Pergamon

Int. J. Heat Mass Transfer. Vol. 40, No. 17, pp. 4229–4238, 1997

Printed in Great Britain
0017–9310/97 $17.00+0.00

PII: S0017–9310(97)00049–5

Steam generation in porous media by volumetric ohmic heating

C. BOUALLOU, G. BUZAN and R. MEYRIGNAC

Ecole Nationale Supérieure des Mines de Paris, Laboratoire Réacteurs et Processus, Groupe Transferts et Vaporisation en Milieux Poreux, 32, Bd Victor, 75015 Paris, France

(*Received* 22 *March* 1994 *and in final form* 14 *October* 1996)

Abstract—A new process is introduced for saturated steam generation in porous media. The process consists of applying an electrical potential between two electrodes in contact with a porous medium (rockwool) impregnated with an ionic solution (water and mineral salts) resulting in a Joule-effect heating. Tap water is fed into the system, introducing soluble salts which increase the conductivity and insoluble salts which modify the porosity. The coupled partial differential equations, derived from the simplified balance equations of energy, motion and diffusion, have been written and solved using a centered finite difference method and are compared favorably to experimental results. The movement of the liquid is modeled using a capillary diffusion of the liquid phase. © 1997 Elsevier Science Ltd.

1. INTRODUCTION

Continuous vaporization of water by ohmic heating in a hydrophilic porous medium has the advantages of volumetric heating, thus causing no fouling of heat exchange surfaces as well as rapid heating rates. Current applications are found in everyday small appliances such as irons, presses and wallpaper strippers, while future applications may include steam boilers and steam generators.

The process consists of applying an alternating electrical potential between two electrodes in contact with a porous medium (rockwool) impregnated with a saline solution. The electrical current passes through the saline solution, heating the water to boiling point and evaporates the solution. Tap water introduces ions which change the system's properties in two ways: the soluble salts add to the electrical conductivity of the liquid, while insoluble salts precipitate, reducing the porosity.

Studies in boiling [1], enhanced heat transfer [2], nuclear waste disposal [3] and methods for enhanced oil recovery contain different elements required for the description of the phenomena. Natural convection in porous media with internal heat sources has been investigated [4] with application to liquid–metal fast breeder reactors. The authors considered a porous bed situated beneath a cooling liquid pool. For the boiling regime, modified Darcy's equations were used to model the vapor and liquid flows. The Joule effect was not considered to vary spatially, rather it was taken as a homogeneous volumetric source term.

A recent review article on statistical and continuum models of fluid–solid reactions in porous media [5] considers the continuous alteration of the pore structure as a result of chemical reactions. This is similar to the precipitation of $CaCO_3$ from hard waters in the process considered here. The classical transport properties in ordered and disordered porous media have been reviewed [6] with emphasis on volume averaging by representing the media as spatially periodic.

The electrical equations involving the Joule effect for heating an ionic fluid flowing in a vertical channel have been derived previously [7]. These authors do not consider phase change nor flow in porous media.

Boiling heat transfer from porous surface layers has been investigated [1, 2] with the desire to enhance the boiling heat transfer using the heat pipe effect; the enhancement due to capillary action has been considered in [8–10], among others.

Steady boiling occurs within the upper section of the porous medium as a result of a dissipation of energy by the Joule effect within the electrical field. Since the porous medium is composed of rigid fibers, no fluidization can occur and no distinctive vapor channels are developed. The steady boiling heat transfer is governed by the nucleate boiling regime, the fibers serving as nucleation sites throughout the volume.

The key phenomena involved in the process are electrical dissipation of energy, phase change, capillarity, permeability, two-phase flow and the diffusion of salts. The salt concentration, saturation, porosity and energy dissipated vary in time. The movement of the liquid phase is modeled with a capillary diffusion coefficient (experimentally determined) and the gradient of the saturation. In this paper a new process for steam generation is described, along with the experimental apparatus used in the investigation and the mathematical model of the coupled transport variables involved.

NOMENCLATURE

A	non-dimensional length
c	concentration [kg m^{-3}]
c_p	concentration in the vertical projection [kg m^{-3}]
D_c	capillary diffusion coefficient [m^2 s^{-1}]
D_s	salt diffusion coefficient [m^2 s^{-1}]
E	electric field [V m^{-1}]
g	gravitational constant [m s^{-2}]
h	height [m]
H	enthalpy [kJ kg^{-1}]
j	current density [A m^{-2}]
K	permeability [m^{-2}]
l	length of porous media [m]
$\dot{m}$	mass flux [kg m^{-3} s^{-1}]
n	index in equation (20)
P	pressure [Pa]
q	energy flux [W m^{-3}]
s	saturation
t	time [s]
T	temperature [K]
U	electrical potential [V]
v	velocity [m s^{-1}]
V	volume [m^3]
x	horizontal coordinate [m]
y	vertical coordinate [m].

Greek symbols

β	non-dimensional coefficient
ε	porosity
φ	salt flux [kg m^{-2} s^{-1}]
μ	viscosity [kg m^{-1} s^{-1}]
ρ	density [kg m^{-3}]
σ	conductivity [S m^{-1}].

Superscripts

b	boiling
c	capillary
eff	effective
is	insoluble
l	liquid
o	initial
p	pore
s	soluble
v	vapor
vap	vaporization.

2. EXPERIMENTAL

Materials

The porous medium employed here was hydrophilic rockwool, a highly porous medium consisting of long, parallel fibers. Rockwool was chosen for its physical characteristics: inflammability, rigidity and relative inertness to attack by chemicals. The porous medium can be characterized by the following parameters: porosity 0.96 ± 0.01, permeability 1.0×10^{-12} m^2, fiber density 2700 kg m^{-3} and apparent density 110 kg m$^{-3} \pm 0.2$.

The porous medium is cut in the form of a 'tee' from a monoblock of rockwool. The upper section is placed entirely within the electrical field while the lower section is immersed in a water tank (Fig. 1). Capillary wicking from the lower saturated-section feeds water to the steam generation zone where the liquid is vaporized.

The construction material for the containment of the porous media was 0.005 m thick polypropylene. It is rigid, inert, electrically insulating and heat resistant up to the temperatures required for the system.

Graphite electrodes (thickness 0.002 m) were chosen to provide the electrical contact along two surfaces of the porous media. The use of graphite avoided oxidation which may occur with metal electrodes such as copper. To avoid hydrolysis an alternating electrical potential (55 V, 50 Hz) was used. The power input to the electrodes determines the overall heat flux to the system.

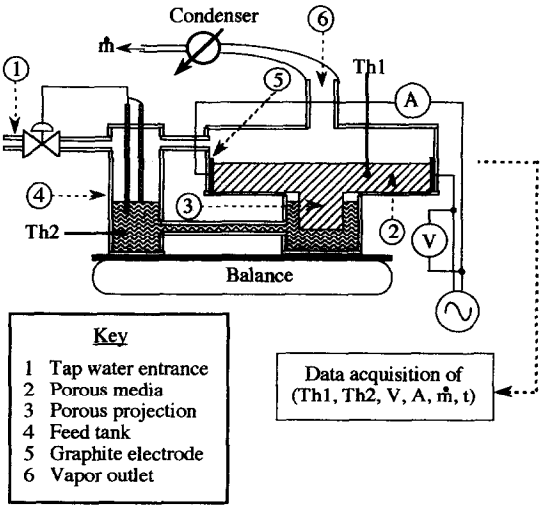

Fig. 1. Scheme of the apparatus.

The porous medium was generally impregnated with a NaCl solution, although any dissociating salt may be used. The salt solution provides a highly conductive electrolyte whose conductivity is minimally changed by the continuous addition of tap water; its composition is given in Table 1.

The feed water contains ions of calcium (Ca^{2+}) and bicarbonate (HCO_3-), which, due to their low solubility product, rapidly form $CaCO_3$(s). The precipitation reduces the porosity, which in turn lowers

Table 1. Tap water composition and properties

Ionic species	Concentration ($mg\,l^{-1}$)	Property	Value
Calcium	112	pH	7.6
Magnesium	6.5		
Sodium	20.0	Conductivity ($\mu S\,cm^{-1}$) at 25°C	528
Potassium	1.5		
Hydrogen carbonate	320		
Chloride	28		
Sulfates	15.7		

the effective conductivity of the system. Other numerous ions remain soluble during the lifetime of the process, increasing the electrical conductivity of the solution.

Apparatus

The experimental apparatus designed and constructed is shown in Fig. 1. The conduction zone was 0.2 m long, 0.03 m high and 0.08 m wide. The two vertical electrodes at both ends have the same surface area as the porous media (0.03×0.08 m). Water preheated to 363.1 K was fed to the center of the conduction zone through a vertical projection of the same width and a height and length of 0.04 m. The porous media was cut from a single block of rockwool, avoiding an interface between the conduction zone and the projection. A constant water level in the reservoir containing this projection ensured a uniform water supply to the conduction zone.

Experiments were conducted under varying initial conditions for a standard duration of 50 h. For each experiment an initial charge of a concentrated salt solution was added to the porous medium to provide the salinity required for the desired power output. Electrical current, voltage and temperature (thermocouple type K) were measured every 15 s during the first hour and then every 15 min for the following 49 h. The system rested on a balance to measure the mass at all times. The steam formed was condensed and collected to determine the production rate. All data except for the rate of condensate production were recorded using a data acquisition system. After each experiment, concentration of soluble salts was determined by measuring the conductivity.

3. FORMULATION OF THE MODEL

In the description of the equations which model the system, we have made some assumptions to reduce the complexity of the problem. The porous media was assumed to be nondeformable, inert and homogeneous. The vapor was assumed to escape the porous media directly after its formation. In using an alternating electrical current, we neglected the possibility of a net migration of ions as well as reactions at the electrodes. We assume the electrical current to be continuous by using the root mean square of the voltage (55 V).

For tap water, we lump the soluble salts together into an equivalent concentration (C_s) of NaCl equal to $0.10\,g\,l^{-1}$ and similarly the insoluble salts (C_{is}), into an effective $CaCO_3$ concentration of $0.27\,g\,l^{-1}$. The small sensible heat change required to raise the temperature to 373.1 K has been neglected before the latent heat requirements.

System definition

The term 'system' is used throughout this paper to describe the ensemble of porous medium, salts, water and steam. The system was modeled as a continuous, vertical medium with steam generation only within the conduction zone. Concentration, velocity, electric field and saturation were considered to evolve in time and position (x, y) and to be constant with respect to the width of the conduction zone.

Initial measurements of the system mass and under steady operating conditions as well as knowledge of the volume of the porous medium allows to determine the liquid saturation when boiling first occurs ($s = 0.8$). This value is used in the expression describing the initial saturation condition.

Operating conditions

Except during the transient stage, the operating temperature within the porous medium is constant and equal to the boiling point of the solution. The operating pressure was constant at 1 atm, the voltage applied was 55 V and the initial concentration of NaCl was $80\,g\,l^{-1}$. At this concentration, the boiling point elevation is 1.1 K, thus the temperature can be assumed constant at 374.1 K. The vapor–liquid equilibrium condition is sustained in all experiments ensuring no superheating of the vapor or porous medium. Neglecting energy losses, the overall energy balance can be written as:

$$q_j = \dot{m}\Delta H_{vap}. \tag{1}$$

Electrical dissipation

The electrical conductivity is a function of the concentration of soluble salts, the temperature and the saturation of water. As shown previously [11]

$$\sigma_{eff} = \sigma_l \varepsilon s^{2.5} \tag{2}$$

represents the effective conductivity for a two-phase media. To account for the changing porosity, we have added the porosity in Ickowski's expression (2). The conductivity and the conductance are related by the ratio of the distance between the electrodes to the surface area.

The presence of the vapor, a non-conducting dispersed phase, lowers the overall electrical conductivity. For example, at a saline concentration of 80 g l^{-1}, unit porosity and a voltage of 55 V, the presence of steam lowers the liquid saturation from 1.0 to 0.8,

lowering the effective conductivity from nearly 120 to 60 mS cm^{-1}.

An empirical correlation [12] accurately gives the conductivity S m^{-1}

$$\sigma_1 = 2.303c^{0.89} \tag{3}$$

at 298 K for a concentration of NaCl between 2 and 100 g l^{-1}. To complete the description of the conductivity, a temperature correction is introduced in which we use a reference temperature of 250 K, corresponding to zero conductivity.

$$\sigma_1(T_b) = \sigma_1(T)\frac{(T_b-250)}{(T-250)}. \tag{4}$$

Thus, given the concentration of NaCl we can calculate the liquid phase conductivity at 298 K using equation (3), correct the liquid phase conductivity for the operating temperature (T_b) and finally account for the porosity and saturation effects (equation (2)) to determine σ_{eff}.

Water: equations of motion and conservation of mass

The saturation (s) of the porous media is defined as the ratio of the volume of the pores occupied by liquid to the volume of pores in a given representative elemental volume:

$$s = \frac{V_1}{V_p}. \tag{5}$$

The velocity of the liquid phase can be expressed by a representation of Darcy's law using a capillary and a gravitational force term. The former is composed of the product of a capillary diffusion coefficient (experimentally determined) and the gradient of the saturation [12, 13].

$$v = -D_c\nabla s + \frac{K}{\mu_1}\rho_1 g. \tag{6}$$

The partial differential equation which expresses the principle of mass conservation for the liquid phase is:

$$-\dot{m} = \rho_1\frac{\partial(\varepsilon s)}{\partial t} + \nabla\cdot(\rho_1 v). \tag{7}$$

Salts: equations of motion and conservation of mass

The soluble salts are transported by the bulk movement of the liquid (convection) and by the forces of diffusion. We write the standard convection/diffusion equation for the flux and the equation expressing the conservation of mass:

$$\varphi = cv - D_s\nabla c \tag{8}$$

$$\frac{\partial c}{\partial t} + \nabla\cdot\varphi = 0. \tag{9}$$

The porosity of the system is assumed to decrease with the precipitation of insoluble salts, principally $CaCO_3$. In this model, a simplified expression (10) for the change in porosity neglecting pore blockage has been taken into account, considered to be locally proportional to the mass of water evaporated.

$$\varepsilon = 1 - \frac{c_{is}\dot{m}}{\rho_{is}\rho_1}t. \tag{10}$$

The change in the porosity is considered only in the equation for the effective conductivity (2). In this expression, the drop in porosity counterbalances the increase in soluble salts, resulting in a relative electrical equilibrium in the system. Since the change in porosity is relatively small (1%) over 50 h of steam vaporization, the porosity is assumed constant and equal to unity in all other equations. This assumption simplifies the equation of motion without introducing excessive uncertainty if the porosity remains greater than 0.9.

Dimensionless equations

We now consider the i and j components (x, y) of the previous equations and we introduce the dimensionless variables listed in Table 2. The three dimensionless groups $(\beta_p, \beta_c, \beta_s)$ are the result of the adimensionalization of the equations [12]. These parameters will be explained thoroughly in Section 4. The equation describing the variation of the voltage and those describing the dissipation of energy becomes:

$$\tilde{\sigma}\left(\frac{\partial^2\tilde{U}}{\partial\tilde{x}^2} + \frac{\partial^2\tilde{U}}{\partial\tilde{y}^2}\right) + \frac{\partial\tilde{\sigma}}{\partial\tilde{x}}\frac{\partial\tilde{U}}{\partial\tilde{x}} + \frac{\partial\tilde{\sigma}}{\partial\tilde{y}}\frac{\partial\tilde{U}}{\partial\tilde{y}} = 0 \tag{11}$$

$$\tilde{E}_x = -\frac{\partial\tilde{U}}{\partial\tilde{x}} \tag{12}$$

$$\tilde{E}_y = -\frac{\partial\tilde{U}}{\partial\tilde{y}} \tag{13}$$

$$\tilde{q}j = \tilde{\sigma}\left[\left(\frac{\partial\tilde{U}}{\partial\tilde{x}}\right)^2 + \left(\frac{\partial\tilde{U}}{\partial\tilde{y}}\right)^2\right] \tag{14}$$

$$\tilde{m} = \tilde{q}. \tag{15}$$

Table 2. Dimensionless variables

$\tilde{x} = \frac{x}{l}$	$\tilde{j} = \frac{j}{\left(\frac{U_0\sigma_0}{l}\right)}$	$\tilde{v} = \frac{v}{\left(\frac{U_0^2\sigma_0}{\rho_1\Delta H_{vap}l}\right)}$
$\tilde{y} = \frac{y}{l}$	$\tilde{t} = \frac{t}{\left(\frac{\rho\Delta H_{vap}l^2}{U_0^2\sigma_0}\right)}$	$\tilde{\varphi} = \frac{\varphi}{\left(\frac{c_0U_0^2\sigma_0}{\rho_1\Delta H_{vap}l}\right)}$
$\tilde{U} = \frac{U}{U_0}$	$\tilde{qj} = \frac{qj}{\left(\frac{U_0^2\sigma_0}{l^2}\right)}$	$\tilde{m} = \frac{\dot{m}}{\left(\frac{U_0^2\sigma_0}{\Delta H_{vap}l^2}\right)}$
$A = \frac{h}{l}$	$\tilde{c} = \frac{c}{c_0}$	$\tilde{E} = \frac{E}{\left(\frac{U_0}{l}\right)}$
$\tilde{c} = \frac{c_p}{c_0}$	$\tilde{\sigma} = \frac{\sigma_{eff}}{\sigma_o}$	$\tilde{S} = s$
$\beta_c = \frac{\rho_1\Delta H_{vap}D_c}{U_0^2\sigma_0}$	$\beta_p = \frac{K\rho_1 gl}{\mu D_c}$	$\beta_s = \frac{D_s\rho_1\Delta H_{vap}}{U_0^2\sigma_0}$

The conservation equations for the liquid and the salt concentration are given by:

$$\frac{\partial \tilde{s}}{\partial \tilde{t}} + \left(\frac{\partial \tilde{v}_x}{\partial \tilde{x}} + \frac{\partial \tilde{v}_y}{\partial \tilde{y}}\right) = -\tilde{m} \tag{16}$$

$$\tilde{v}_x = -\beta_c \frac{\partial \tilde{s}}{\partial \tilde{x}} \tag{17}$$

$$\tilde{v}_y = -\beta_c \left(\beta_p + \frac{\partial \tilde{s}}{\partial \tilde{y}}\right) \tag{18}$$

$$\frac{\partial \tilde{c}}{\partial \tilde{t}} - \beta_s \left(\frac{\partial^2 \tilde{c}}{\partial \tilde{x}^2} + \frac{\partial^2 \tilde{c}}{\partial \tilde{y}^2}\right) + \tilde{v}_x \frac{\partial \tilde{c}}{\partial \tilde{x}} + \tilde{v}_y \frac{\partial \tilde{c}}{\partial \tilde{y}} + \left(\frac{\partial \tilde{v}_x}{\partial \tilde{x}} + \frac{\partial \tilde{v}_y}{\partial \tilde{y}}\right)\tilde{c} = 0. \tag{19}$$

In the process under investigation, the walls form impermeable boundaries to the liquid and salt motion which are also electrically isolating. The saturation is constant at the inlet for the liquid and the normalized voltage is constant at the electrodes. The initial condition for the saturation follows from an initial zero velocity condition. The concentration is normalized to the initial concentration throughout the porous medium.

The concentration in the vertical projection ($\tilde{c}_p$) is determined by treating its volume like a continuous stirred tank reactor with an initial concentration $\tilde{c}_{po} = 0.33$. This concentration was determined by allowing the process to reach the boiling point and immediately cutting all the power, removing the projection and measuring the conductivity of the liquid contained in the volume. This concentration serves as a boundary condition at the interface defined by $\tilde{y} = 0.0$ and $0.4 < \tilde{x} < 0.6$. The boundary and initial conditions are shown in Fig. 2.

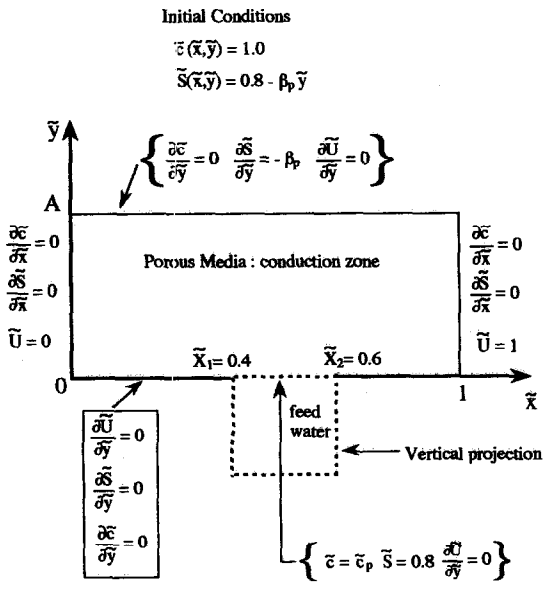

Fig. 2. Boundary and initial conditions for the dimensionless system in the X–Y plane.

Solution method

An implicit predictor/corrector centered finite difference method was employed to solve the system of coupled differential equations subject to the boundary and initial conditions given above and shown in Fig. 2. The implicit method ensures stability for the system of equations. A rectangular grid size of 41 points in the $\tilde{x}$-direction and 11 in the $\tilde{y}$-direction was implemented. The horizontal ($\tilde{x}$) coordinate is privileged by using more gridpoints due to the difference between the length (0.2 m) and the height (0.03 m) of the conduction zone.

The initial values for the saturation, porosity and NaCl concentration are considered at the boiling point of the fluid [equation (2)] to determine the effective conductivity. The system of equations is solved in two steps, then first being the resolution of the electrical equations (11)–(15) and the second being the equations of motion and conservation (16)–(19).

Step one uses the initial conditions to find a steady-state solution to the second-order equation in the voltage (11) and evaluates the energy flux. For every step in time $\tilde{t}$, a steady-state solution is found by iterating upon an index (n). A flowsheet for the solution method is given in Fig. 3.

The step size for the adimensional time ($\tilde{t}$) was chosen to be 5.0×10^{-4}, a compromise which is large enough to limit round-off error and also sufficiently small for convergence of the small grid size. Equation (11) is iterated upon until a criteria of convergence is met, given by:

$$\mathrm{MAX}_{(i,j)} \left| \frac{U_{i,j}^{n+1} - U_{i,j}^{n}}{U_{i,j}^{n}} \right| \leqslant 5.0 \times 10^{-7} \tag{20}$$

where $U_{i,j}^{n}$ is the voltage at point (i,j) and at an iteration time (n).

The mass of water evaporated is, thus, calculated at each node and assumed constant within each corresponding volume defined by the grid size ($\Delta\tilde{x} \times \Delta\tilde{y}$). An equivalent volume to the total water evaporated in $\Delta\tilde{t}$ is added to the vertical projection volume and the resulting concentration ($\tilde{c}_p$) is recalculated.

With the energy flux resolved at time $\tilde{t}$, the second step is to solve the equations of motion (16)–(18) and the salt flux (19) using the same implicit method. For every time $\tilde{t}$, the results of the second step are used as the new conditions for the concentration, porosity and saturation to resolve equation (11).

4. RESULTS

Model validation

Using the parameters for the experimental comparison in Table 3, a simulation of 50 h of continuous operation was made and compared with experimental results. We compare the model predictions to the measurements for three different quality feed waters, deionized, tap water and a 1.0 g l^{-1} NaCl solution. Measurements of the electrical current at a voltage of

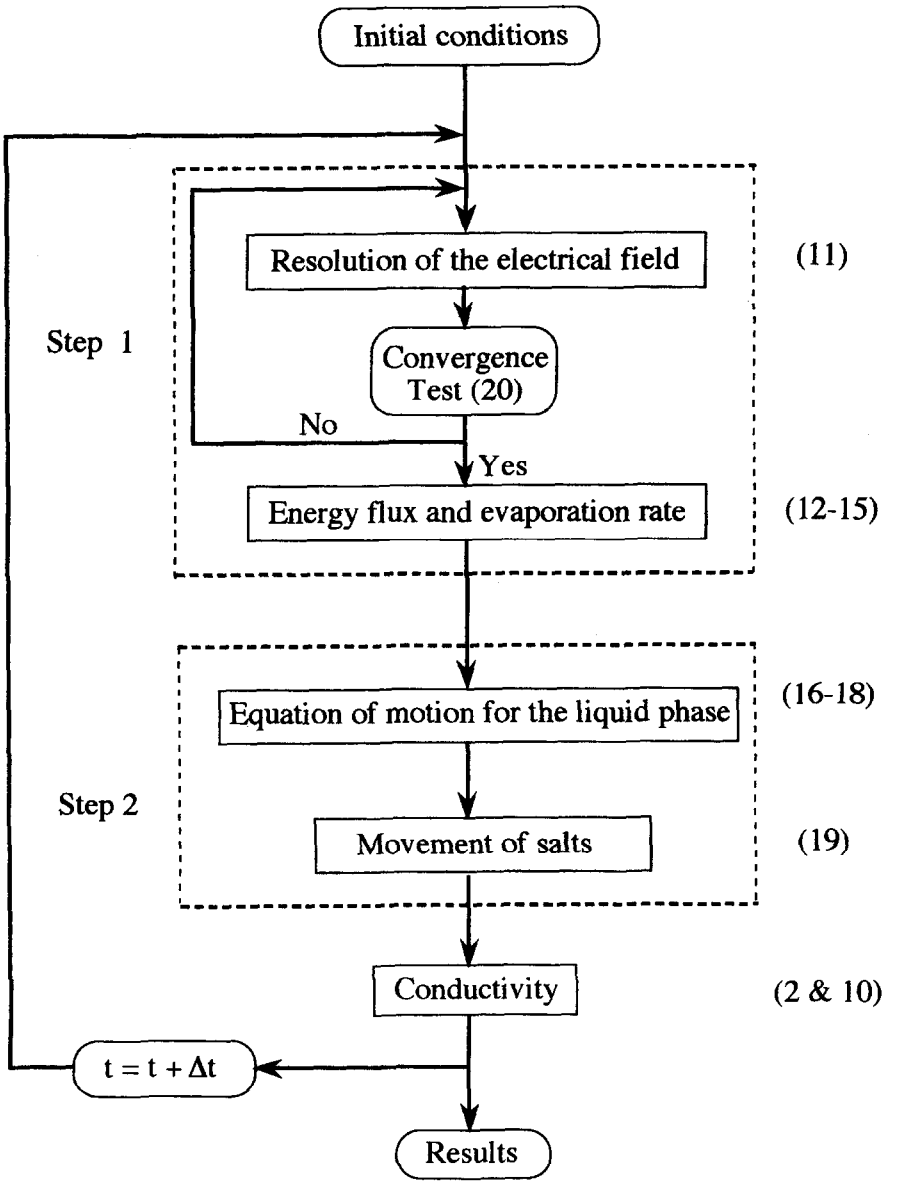

Fig. 3. Solution flowsheet for equations (10)–(19).

55 V and for an initial salt concentration of 80 g l^{-1} were taken during 50 h.

The model accurately predicts (Fig. 4) the electrical current during this period. Using tap water, the intensity is seen to slowly rise due to the accumulation of soluble salts in the water being more influential on the conductivity than the reduction of the porosity due to precipitation.

To further show the effect of salts on the system, pure water and a 1 g l^{-1} NaCl solution were used as feed water. As expected, the model and experimental results show no change in the intensity for the case of a pure water feed, showing that the system is invariant if deionized water is used. In using a feed of 1 g l^{-1} NaCl, the model predicts an increase in intensity from 8 to 13.5 A during the same time period, due to the strong increase in salinity. The prediction is slightly higher than the experimental results due to heat losses which occur at higher power levels. The loss of heat from the apparatus renders it less efficient, therefore less water is vaporized and the concentration of salts is lower for all times greater than zero.

The model correctly predicts the concentration of NaCl over time as a function of position. Comparison to experimental results for the case of a tap water feed are presented in Fig. 5. The porous media was cut in two along the vertical axis and then into five pieces each measuring 4 cm in length, 8 in width and 1.5 in height. The concentration reported in Fig. 5 is the average concentration in each sample. The uncer-

Table 3. Model parameters used in parametric studies except as indicated

Parameter	Value
Distance between electrodes	0.200 m
Height	0.030 m
Width	0.080 m
Width of porous projection	0.040 m
Initial concentration in conducting zone	80.0 g l^{-1}
Feed concentration of soluble salts	0.10 g l^{-1}
Feed concentration of insoluble salts	0.27 g l^{-1}
Initial saturation at porous projection interface	0.80
Voltage	55 V
β_p	0.457
β_c	0.650
β_s: for experimental comparison	0.0665
β_s: for parametric analysis	0.0152

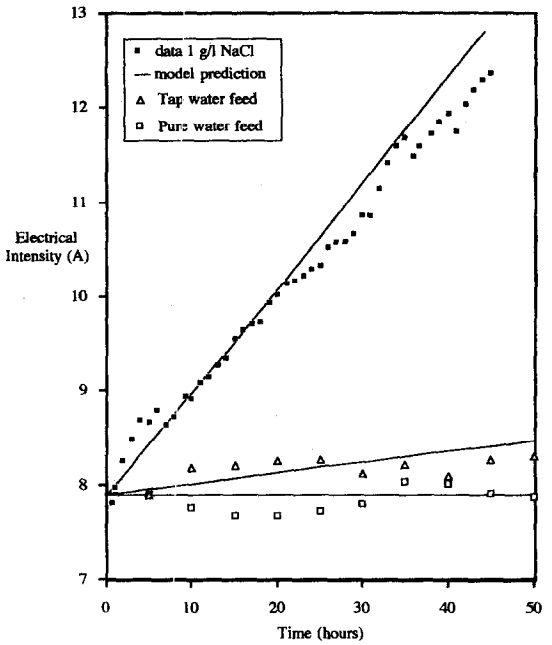

Fig. 4. Comparison of model predictions with experimental results for differing feed waters: initial NaCl concentration 80 g l^{-1}, voltage 55 V.

tainty in the measurements is due to liquid movement during the sectioning process. The average standard deviation for the concentration was determined to be 10% in a series of six experiments designed to test the repeatability of the experiment.

The 'V' shape to the curve is due to the net convective movement in the porous media. Feed water enters from the projection and rises while moving laterally towards the electrodes. The movement convects the salt, forming the gradient.

The model does not agree with the experimental measurements near the electrodes. This discrepancy is believed to be due to a density effect of the fluid, as a matter of fact, not considered in the model. Near the electrodes, the model predicts a concentration independent of height. We interpret this as an average

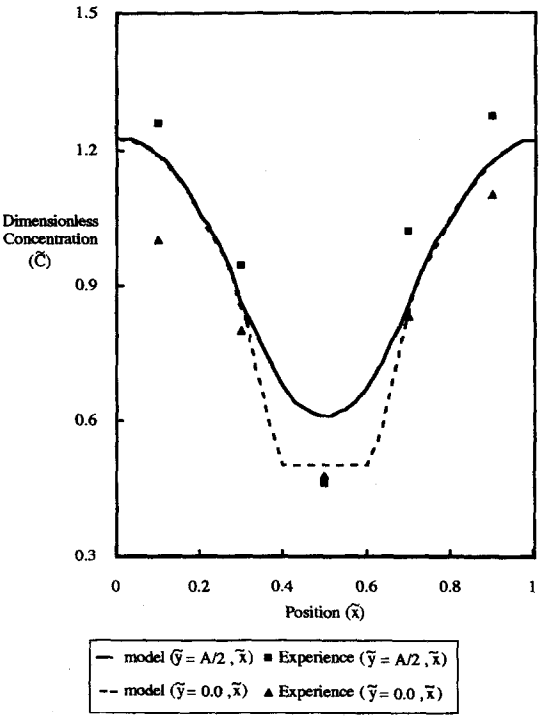

Fig. 5. Experimental results and model predictions of the dimensionless concentration for the middle (y = 1.5 cm) and bottom (y = 0.0 cm) planes in the porous medium. Initial NaCl concentration 80 g l^{-1}, voltage 55 V.

concentration, falling between the experimental concentration at $\tilde{y} = 0$ and $\tilde{y} = A/2$.

Parametric study

In the development of the model, we have formed three dimensionless groups (Table 2): β_p, β_c and β_s [12]. These parameters have significant effects on the relative contributions of capillarity, gravity, permeability and diffusion. Using the finite difference model, we show the effects of these three groups on the mass of water evaporated, the saturation distribution and the concentration of soluble salts. The model parameters given in Table 3 are used as a basis for comparison and the results depicted in Figs. 6–10 are given for the plane defined by $0 < \tilde{x} < 1$ and $\tilde{y} = A/2$.

β_p represents the product of the permeability and gravity with respect to the effect of the capillary diffusion (Table 2). This parameter directly influences the initial saturation distribution.

β_p has little effect on the saturation in the horizontal direction but a change in β_p from 0.001 to 1.0 changes the saturation gradient in the vertical plane ($\tilde{x} = 0.5$, $0 < \tilde{y} < A$) as can be seen by equation (18).

In lowering the saturation, the electrical dissipation and the mass of evaporated water is reduced. Figure 6 shows the change in the evaporation rate as a function of position ($\tilde{x}$) to be symmetric along the central axis, $\tilde{x} = 0.5$. This is expected, considering the boundary condition for the saturation, $s = 0.8$ for $\tilde{y} = 0$ and

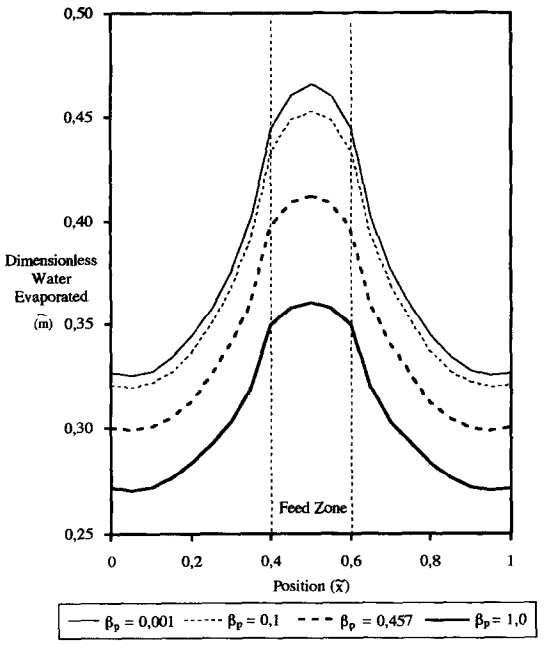

Fig. 6. Parametric study of the permeability parameter β_p on the quantity of water evaporated after 50 h of simulation. Initial NaCl concentration 80 g l^{-1}, feedwater NaCl concentration (C_s) 0.10 g l^{-1}, feedwater $CaCO_3$ concentration (C_{is}) 0.27 g l^{-1}, voltage 55 V, $\beta_c = 0.65$, $\beta_s = 0.0152$.

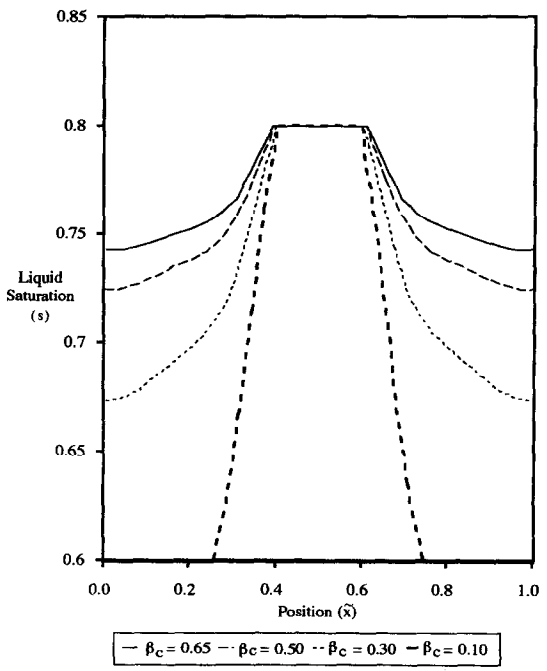

Fig. 7. Parametric study of the adimensional diffusion coefficient β_c on the saturation after 50 h of simulation. Initial NaCl concentration 80 g l^{-1}, $C_s = 0.10$ g l^{-1}, $C_{is} = 0.27$ g l^{-1}, voltage 55 V, $\beta_p = 0.457$, $\beta_s = 0.0152$.

$0.4 < \tilde{x} < 0.6$, representing the symmetric feed water zone.

It can be seen that, as β_p is increasingly reduced, capillary forces dominate the gravitational contribution, and the curves approach limiting value. This is the case for a very large flat porous media whose capillary forces control the liquid movement, and gravity can be most likely ignored. This parameter has a minimal effect on the NaCl concentration; however, since the precipitation is assumed proportional to the vaporization of water, changing β_p also influences the porosity distribution in an analogous way to the mass flux of evaporated water.

β_c fixes the contribution of the capillary diffusion coefficient in the equations of motion (19), (20). The velocity of the liquid phase is modeled using a capillary diffusion coefficient and a driving force, the gradient of the saturation. Figure 7 shows that a lowering of β_c results in a dryout of the porous media.

For $\beta_c = 0.1$ the saturation is insufficient for the electrical continuity, a 'dryout' occurs after 10 h at the two sides of the porous medium at $\tilde{x} = 0$ and $\tilde{x} = 1$. The liquid dryout is caused by the reduced capacity of the capillary forces. The rate of evaporation is higher than the rate of liquid replenishment by liquid diffusion and capillary forces, thus the dryout occurs at the ends.

The electrical current density decreases as well due to the diminution of the liquid saturation, thus the effective electrical conductivity. Since the effective electrical conductivity is proportional to the saturation raised to the 2.5 power [equation (2)], a small change in the saturation leads to a large change in the electrical current. Thus, we find that our system is very sensitive to this parameter.

The last parameter defined is β_s which is proportional to the salt liquid phase diffusion coefficient. In changing β_s, the relative contribution to the motion of the salts is changed between the convective and diffusive terms in the flux equation (19). Figure 8 shows that the effect of increasing this coefficient is to reduce the concentration gradient, resulting in a more homogeneous evaporation. Large values for β_s result in a fast diffusion of salts.

When the diffusion is limited (small β_s), the concentration is very low near the entrance due to the arrival of feed water at a lower concentration. This causes a nonuniformity of the electrical field, the electrical resistance being relatively strong in the center and weak near the electrodes.

The saturation distribution as a function of $\tilde{x}$ at the same conditions as in Fig. 8 is shown in Fig. 9. The saturation decreases towards an asymptotic limit with an increase in β_s as a secondary result of the change in the concentration distribution. We find no difference in the saturation gradient for β_s larger than 0.152. The concentration distribution influences the electrical conductivity and, therefore, the electrical field ($\tilde{E}$) and the local rate of evaporation.

The net effect on $\tilde{E}$ due to the saturation and concentration influences is quite interesting. In Fig. 10, we show the a-dimensional electric field using the previous conditions and $\beta_s = 0.015$, 0.066, 0.15 and 1.0. The results show a decrease in the electrical field at

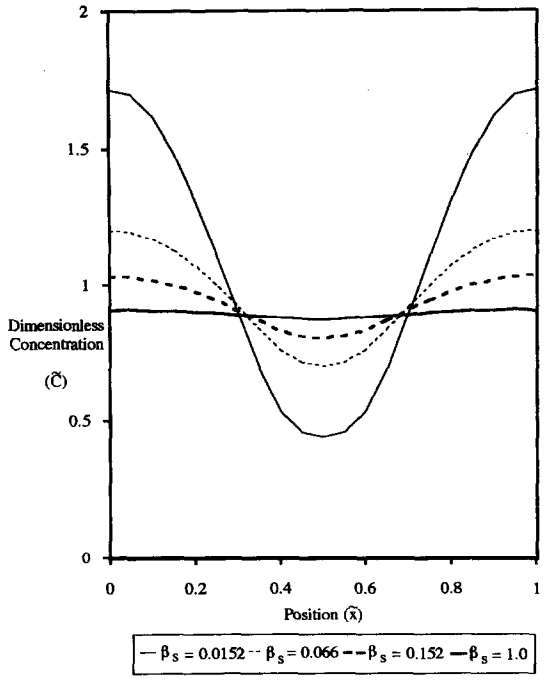

Fig. 8. Parametric study of the adimensional parameter β_s on the concentration after 50 h of simulation. Initial NaCl concentration 80 g l^{-1}, $C_s = 0.10$ g l^{-1}, $C_{is} = 0.27$ g l^{-1}, voltage 55 V, $\beta_p = 0.457$, $\beta_c = 0.65$.

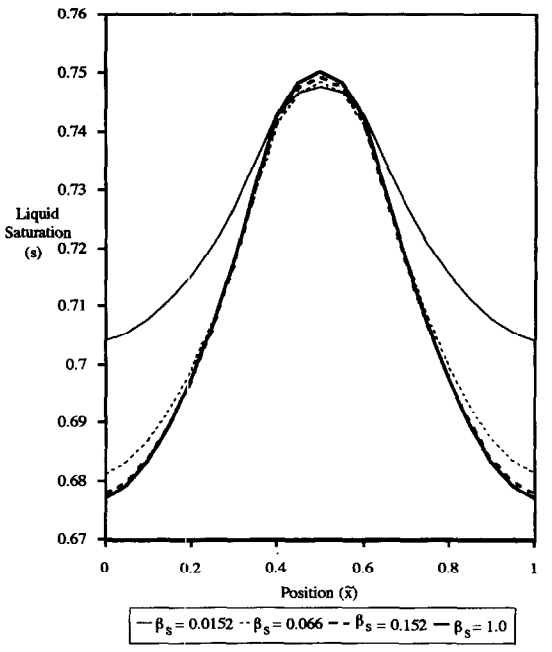

Fig. 9. Parametric study of the adimensional parameter β_s on the saturation after 50 h of simulation. Initial NaCl concentration 80 g l^{-1}, $C_s = 0.10$ g l^{-1}, $C_{is} = 0.27$ g l^{-1}, voltage 55 V, $\beta_p = 0.457$, $\beta_c = 0.65$.

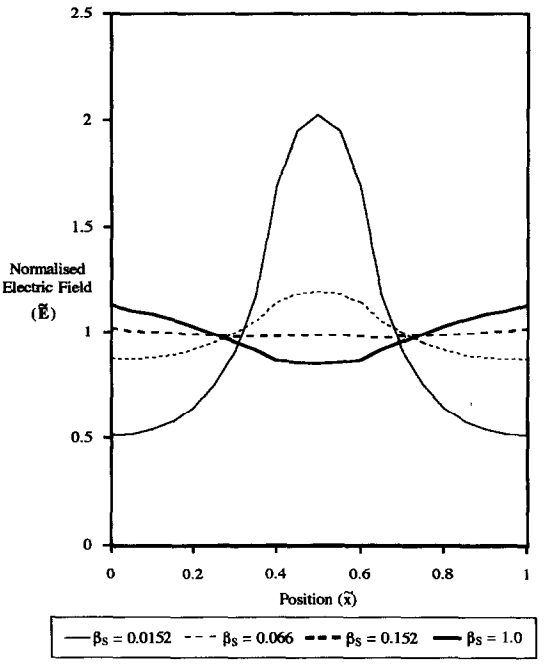

Fig. 10. Parametric study of the adimensional parameter β_s on the electric field strength after 50 h of simulation. Initial NaCl concentration 80 g l^{-1}, $C_s = 0.10$ g l^{-1}, $C_{is} = 0.27$ g l^{-1}, voltage 55 V, $\beta_p = 0.457$, $\beta_c = 0.65$.

the center and then a reversal of $\tilde{E}$ due to changes in the concentration distribution and the saturation.

The electrical field is proportional to the inverse of the effective conductivity (8). For $\beta_s = 0.015$ the concentration is very strong near electrodes and low at the center while the saturation varies inversely. The strong change in the concentration dominates the conductivity and thus the electrical field resembles the concentration.

As β_s increases (0.15) the concentration gradient is

reduced and the saturation gradient is increased. These changes have an overall effect of cancelation, the effective conductivity and, thus, the electrical field are found to be relatively constant (Fig. 10).

As β_s is increased further ($\beta_s = 1.0$), the electrical field reverses upon itself. At this point the concentration is nearly constant and the saturation gradient is identical to the case of $\beta_s = 0.15$. The overall effect on $\tilde{E}$ is, therefore, determined by the saturation distribution. Under these conditions, the production of steam is found to be greater near the electrodes than at the center of the porous medium.

5. CONCLUSIONS

In this paper, we have described the ohmic heating of a saline solution in a porous media (hydrophilic rockwool) for steam generation. The equations of energy, of motion and of salt diffusion have been written and solved using a centered finite difference method. The movement of the liquid is modeled using a capillary diffusion of the liquid phase.

The model is favorably compared to experimental results for 50 h of operation using tap-water, purified water and a 1 g l^{-1} saline solution. The relative contribution of the permeability, gravity, capillarity and diffusion forces are considered in a parametric study of three dimensionless groups. The conditions for dry-out of the porous bed are determined as a limiting case for the validity of the model.

The saturation diffusion coefficient (β_s) has been shown to influence the saturation and salt concentration distributions and, thus, the electrical field. It has been shown that for large β_s, a reversal of the electrical field can occur resulting in a stronger dissipation of energy in the vicinity of the electrodes.

REFERENCES

1. Lu, S. M. and Chang, R. H., Pool boiling from a surface with a porous layer. *AlChE Journal*, 1987, **33**(11), 1813–1828.
2. Afgan, N. H., Jovic, L. A., Kovalev, S. A. and Lenykov, V. A., Boiling heat transfer from surfaces with porous layers. *International Journal of Heat and Mass Transfer*, 1985, **28**(2), 415–422.
3. Doughty, C. and Pruess, K., A similarity solution for two-phase fluid and heat flow near high-level nuclear waste packages emplaced in porous media. *International Journal of Heat and Mass Transfer*, 1990, **33**(6), 1205–1222.
4. Hardee, H. C. and Nilson, R. H., Natural convection in porous media with heat generation. *Nuclear Science and Engineering*, 1976, **63**, 119–132.
5. Sahimi, M., Gavalas, G. R. and Tsotis, T. T., Statistical and continuum models of fluid–solid reactions in porous media. *Chemical Engineering Science*, 1990, **45**(6), 1443–1502.
6. Quintard, M. and Whitaker, S., Transport in ordered and disordered porous media: volume-averaged equations, closure problems and comparison with experiment. *Chemical Engineering Science*, 1993, **48**(14), 2537–2564.
7. Ould El Moctar, A., Peerhossaini, H., Le Peurian, P. and Bardon, J. P., Procédé de chauffage volumique d'un liquide par conduction électrique directe. *Revue Générale de Thermique*, 1991, **360**, 747–755.
8. Udell, K. S., Heat transfer in porous media heated from above with evaporation, condensation and capillary effects. *Journal of Heat Transfer, Transactions of the ASME*, 1983, **105**, 485–492.
9. Udell, K. S., Heat transfer in porous media considering phase change and capillarity—the heat pipe effect. *International Journal of Heat and Mass Transfer*, 1985, **28**(2), 485–494.
10. Stubos, A. K., Satik, C. and Yortsos, Y. C., Effects of capillary heterogeneity on vapor–liquid counterflow in porous media. *International Journal of Heat Mass Transfer*, 1993, **36**(4), 967–976.
11. Iczowski, R. P., Electrical conductivity of partially saturated porous solids. *Industrial Engineering Chemical Fundamentals*, 1970, **9**(4), 674–676.
12. Meyrignac, R., Etude de la vaporisation de l'eau chauffée volumiquement par effet Joule en milieu poreux: application à la laine de roche pour des eaux de qualités differentes. Ph.D. thesis, Ecole Nationale Supérieure des Mines de Paris, Paris, 1993.
13. Wang, B. X. and Fang, Z. H., Water absorption and measurement of the mass diffusivity in porous media. *International Journal of Heat and Mass Transfer*, 1988, **31**(2), 251–257.

APPENDIX

In the following, we develop the Maxwell's equations describing ohmic heating. The system was modeled as a continuous conducting media with an effective conductivity (σ_{eff}), defined by equation (2).

$$\nabla \cdot j = 0 \tag{A1}$$

$$[\nabla \times E] = 0 \tag{A2}$$

$$j = \sigma_{eff} E \tag{A3}$$

$$q = [j : E]. \tag{A4}$$

We see from equation (A4) that the energy dissipated (q) is equal to the scalar product of the courant density (j) and the electric field (E). The electric field is equal to the negative gradient of the electrical potential. The following equations result.

$$E = -\nabla U \tag{A5}$$

$$\nabla \cdot (\sigma_{eff} \nabla U) = 0 \tag{A6}$$

$$q = \sigma_{eff} \nabla^2 U. \tag{A7}$$